

# Microstructure and Oxidation-Resistant Property of Sol-Gel-Derived $ZrO_2$ - $Y_2O_3$ Films Prepared on Austenitic Stainless Steel Substrates

Kun'ichi Miyazawa\*

Department of Materials Science, Faculty of Engineering, The University of Tokyo, Tokyo, 113, Japan

Kunio Suzuki

The Institute for Solid State Physics, The University of Tokyo, Tokyo, 106, Japan

Myeong Yong Wey

Department of Materials Science, Chung-Buk University, Chong-Ju, Korea

The effect of  $Y_2O_3$  addition to the oxidation resistance of sol-gel-derived zirconia films coated on austenitic stainless steel substrates was examined. The oxidation weight gain measurement and XRD analyses of oxides showed that addition of  $Y_2O_3$  reduces oxide formation. TEM observations revealed that the films are joined to the substrates via an amorphous layer with concentrated Si, and the layer grew thicker by adding  $Y_2O_3$  or elevating the firing temperature. Lattice constants of the films were shown to be more expanded than the zirconia powders prepared from the coating liquids.

## I. Introduction

ZIRCONIA is widely used for the surface modification of metals. Fabrication of zirconia ( $ZrO_2$ ) coatings for stainless steels through sol-gel processing has been reported by several authors. Using zirconium tetraoctylate, Izumi *et al.*<sup>1</sup> examined the oxidation protectiveness of pure zirconia films coated on SUS304 stainless steel. They showed that the oxidation weight gain was reduced by increasing the coating thickness. Shane and Mecartney<sup>2</sup> prepared a  $ZrO_2$ -8 wt%  $Y_2O_3$  film on 446 stainless steel by using zirconium tetrabutoxide and showed that the sol-gel-derived zirconia film worked effectively for protection from acids.

From the viewpoint of high-temperature oxidation, the chemical composition of the coated film is very important, because  $ZrO_2$ - $Y_2O_3$  is a well-known solid electrolyte which transports oxygen ions at a high temperature, and the conductivity of oxygen ions is known to vary drastically, depending on the  $Y_2O_3$  content.<sup>3</sup> As the high-temperature oxidation is caused by the flow of oxygen ions and electrons through the oxide scales, the oxidation resistance of  $ZrO_2$ - $Y_2O_3$  films is expected to change with their chemical composition.

In this paper, the effect of yttria ( $Y_2O_3$ ) addition on the oxidation behavior of the stainless steel substrates coated with the sol-gel-derived zirconia films is studied through the measurement of oxidation weight gain and the X-ray diffraction (XRD)

analysis of formed oxides. The films subjected to the oxidation experiment are also investigated by XRD and compared with the powders obtained from the same coating liquids in order to reveal their microstructural characteristics that are caused by the bonding and oxidation. In addition, the structure of the films and film-substrate interfaces is examined in relation to the oxidation resistance by using the high-resolution transmission electron microscope (HRTEM), TEM-EDX, and XRD analyses which are reported.

## II. Experimental Procedure

Coating liquids were prepared using zirconium tetra *n*-propoxide ( $Zr(O-n-C_3H_7)_4$ , Soekawa Chemicals, Japan), yttrium acetate tetrahydrate ( $Y(CH_3COO)_3 \cdot 4H_2O$ , Soekawa Chemicals) and *n*-propyl alcohol (as-received, water content 0.3% max). Zirconium tetra *n*-propoxide and yttrium acetate tetrahydrate were separately dissolved in *n*-propyl alcohol in air and mixed with a magnetic stirrer for several hours in a 100-mL beaker with a plastic film seal until a transparent solution was obtained. The liquid concentration was fixed to be 0.1M  $ZrO_2$ - $x$  mol%  $YO_{1.5}$  ( $x = 0$  to 30).

Austenitic stainless steel (SUS304) substrates (15 mm  $\times$  15 mm  $\times$  1 mm) were annealed under vacuum at 900°C for 2 h, and both surfaces were mechanically polished with SiC paper and mirror-polished using 1.0- and 0.3- $\mu$ m alumina powders. The zirconia sol was dip-coated on the substrates, with a withdrawal speed of 1.0 mm·s<sup>-1</sup> at room temperature (20°-22°C) in air. The relative humidity of the room was kept in the range of 40%-50%. The dip-coating was repeated 10 times in each substrate for the oxidation experiment. After each dip, the substrates were dried for 30 s. Next, the substrates dip-coated 10 times were dried in air at 110°C for 0.5 h, fired at 900°C for 2 h under vacuum with a heating rate of 200°C·h<sup>-1</sup>, and oxidized at 900°C for 1 h in air. The weight gain measurement was done using two to four specimens for each composition 10 min after the completion of substrate cooling.

The film thickness of the coatings was estimated by the step height measurement with stylus method (Talystep, Rank Taylor Hobson<sup>4</sup>) using silica ( $SiO_2$ ) glass substrates with pure zirconia coatings. In preparing powders, the coating liquids were evaporated at 70°C under vacuum and dried at 150°C. The dried gels were pulverized in an alumina mortar and fired at 900°C for 3 h in air with a heating rate of 200°C·h<sup>-1</sup> and then furnace-cooled.

A strong-beam X-ray diffractometer (MAC MXP-18, 40 kV, 200 mA,  $CuK\alpha$  radiation) and transmission electron microscopes (Hitachi H-9000 (300 kV), JEOL 2000 FX (200 kV) with EDX systems (Tracor Northern)) were used in the microstructural analysis. Lattice constants measurement of the powders by XRD was done using 400 and 004 peaks as has been

R. E. Loehman—contributing editor

Manuscript No. 193719, Received March 28, 1994; approved July 27, 1994.  
Presented in part at the 95th Annual Meeting of the American Ceramic Society, Cincinnati, OH, April 22, 1993 (Basic Science, Electronics and Engineering Ceramics Division, Paper No. SXVI-41-93) and at the 7th International Conference on Surface Modification Technologies (SMT 7), Sanjo, Niigata, Japan, November 2, 1993.  
\*Member, American Ceramic Society.

reported by Yoshimura *et al.*<sup>5</sup> The measurement of lattice constants was done five to six times for each composition. The (111) plane spacing of the films was measured for each composition, using five to six samples. Si was used as an internal standard. Integrated intensity measurement of 111 reflections from monoclinic, tetragonal, and cubic phases of zirconia films was done using four to seven samples in each composition. In the peak intensity measurement of the oxidized specimens by XRD, two to three samples for 111 reflections from the SUS304 substrates, three to seven samples for 104 reflections from  $(\text{Fe}_{0.6}\text{Cr}_{0.4})_2\text{O}_3$ , and two to four samples for 400 and 711 reflections from  $\text{FeCr}_2\text{O}_4$  were analyzed in each composition.

Surface observation of the specimens was done by EPMA (Shimadzu 8705). In the cross-sectional observation of coatings by HRTEM, the specimens were sliced with a resinoid blade, polished with diamond powders (0.25–9  $\mu\text{m}$ ) and ion-milled (model 600, Gatan). In the TEM-EDX analysis, an electron probe 10 nm in diameter was used. A program for the standardless quantitative analysis was used in the measurement of film composition.

### III. Results

#### (1) Estimation of the Thickness of $\text{ZrO}_2\text{-Y}_2\text{O}_3$ Films

Figure 1 shows the thickness of pure zirconia films on  $\text{SiO}_2$  substrates evaluated by the step height measurement. The film thickness increases linearly by repeating the coating times. A thickness of 6 nm is shown to be obtained by one coating process. Figure 2 shows the integrated intensities of 111 reflections from the films prepared on the stainless steel substrates after the oxidation experiment. The intensity measurement of each sample was done using the same diffraction condition. According to the theory of X-ray diffraction, intensity  $I$  from a specimen with a thickness  $t$  and crystal grains with a random orientation is expressed as follows:<sup>6</sup>

$$I = \text{const.} \int_0^t FF^* \exp(-2\mu z/\sin \theta) dz \quad (1)$$

where  $F$  is the crystal structure factor,  $t$  the film thickness,  $\mu$  the linear absorption coefficient, and  $\theta$  the angle of incidence. According to Ingel and Lewis,<sup>7</sup> the density  $\rho$  ( $\text{kg}/\text{m}^3$ ) of cubic  $\text{ZrO}_2\text{-Y}_2\text{O}_3$  varies as

$$\rho = (818.435 - 137.023M/(100 + M))(1/d_0^3) \quad (2)$$

where  $M$  is the mole percentage of  $\text{Y}_2\text{O}_3$  and  $d_0$  (nm) is the cubic lattice constant. From this equation, the linear absorption coefficient is calculated as  $670.1 \text{ cm}^{-1}$  (0 mol%  $\text{YO}_{1.5}$ ) to  $629 \text{ cm}^{-1}$  (30 mol%  $\text{YO}_{1.5}$ ). Assuming the film thickness of 60 nm for a film with 10 coating layers, the lattice constant of 0.5145 nm for  $\text{ZrO}_2\text{-20 mol% YO}_{1.5}$ ,<sup>7</sup> and using  $\lambda = 0.15405 \text{ nm}$  for  $\text{CuK}\alpha$  radiation, the value  $(2\mu z/\sin \theta)$  in Eq. (1) is estimated at 0.03.

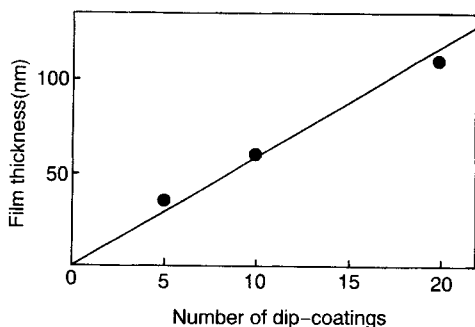


Fig. 1. Relationship between the thickness of pure zirconia films coated on  $\text{SiO}_2$  substrates and the coating times.

This value is very small; then, for a thin film, Eq. (1) can be approximated as

$$I = \text{const.} FF^* t \quad (3)$$

i.e., the intensity varies in proportion to the film thickness. Since the structure factor,  $\theta$ , and the absorption coefficient remain almost constant in the tetragonal and cubic zirconia of this study, the intensity of 111 reflections is proportional to the film thickness. Therefore, in Fig. 2, the film thickness is found to vary with  $\text{Y}_2\text{O}_3$  content, taking the maximum value at 14 mol%  $\text{YO}_{1.5}$  and decreasing with increasing  $\text{Y}_2\text{O}_3$  content. The film thickness changes by a factor of approximately two in the whole compositional range of the present study.

#### (2) Oxidation Behavior of Zirconia-Coated Specimens

The weight gain of the SUS304 substrates with  $\text{ZrO}_2\text{-Y}_2\text{O}_3$  films after oxidation at  $900^\circ\text{C}$  for 1 h is shown in Fig. 3. The weight gain is found to change with the  $\text{Y}_2\text{O}_3$  content and has a general trend of decreasing with increasing  $\text{Y}_2\text{O}_3$  content. This result shows that the compositional factor must be considered in order to obtain an excellent oxidation-resistant coating. Examples of surface observation of the specimens are shown in Fig. 4 for  $\text{ZrO}_2\text{-15 mol% YO}_{1.5}$  thin films coated on the SUS304 substrates. A uniformly coated surface can be seen in photo (a). In photo (b), the film surface is seen to become granular from the

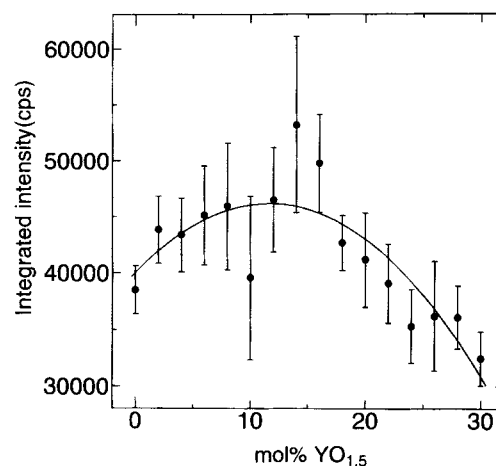


Fig. 2. XRD integrated intensities of the 111 reflections from  $\text{ZrO}_2\text{-Y}_2\text{O}_3$  films. The values are the summation of the reflection intensities from the monoclinic, tetragonal, and cubic phases ( $111_m + 111_c + 111_t + 111_c$ ).

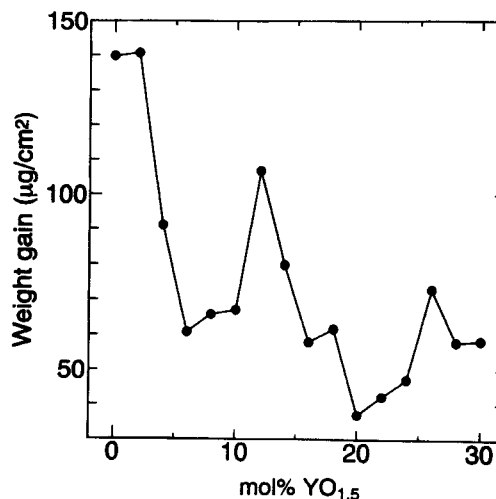
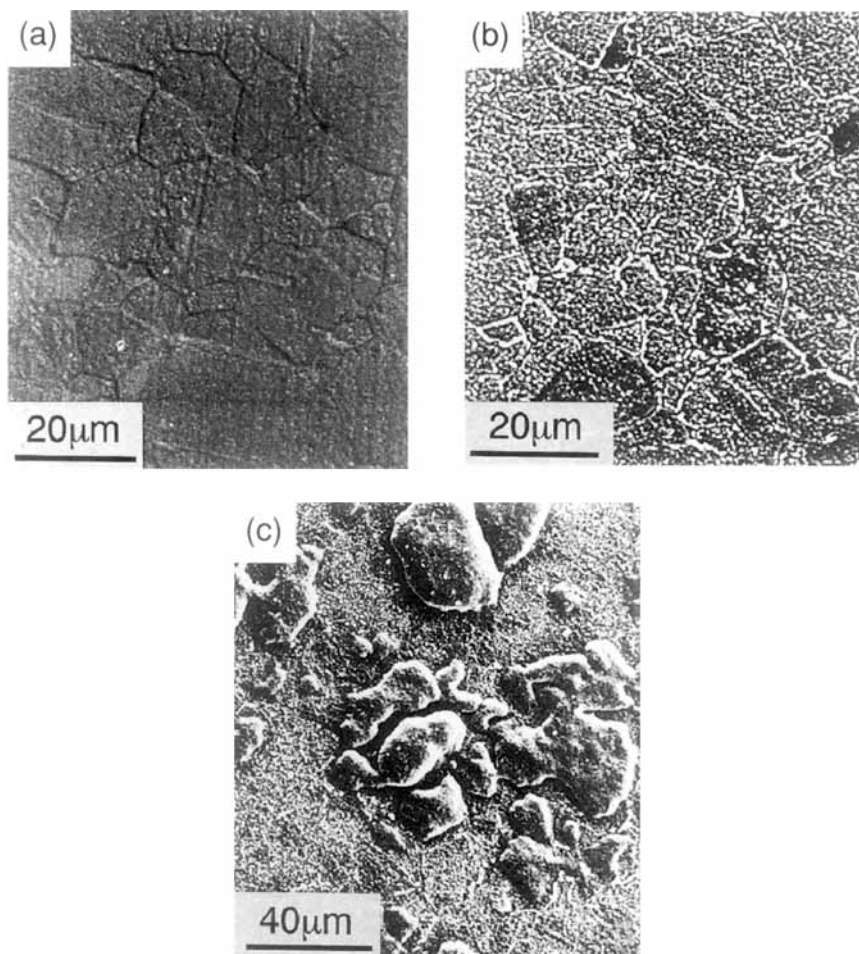


Fig. 3. Weight gains of the SUS304 substrates with  $\text{ZrO}_2\text{-Y}_2\text{O}_3$  coatings oxidized at  $900^\circ\text{C}$  for 1 h in air.



**Fig. 4.** (a) SEM image of a  $ZrO_2$ -15 mol%  $YO_{1.5}$  film coated on a SUS304 substrate fired at  $900^\circ C$  for 2 h under vacuum. (b) SEM image of a  $ZrO_2$ -15 mol%  $YO_{1.5}$  film coated on a SUS304 substrate fired at  $900^\circ C$  for 2 h under vacuum and oxidized at  $900^\circ C$  for 1 h in air. (c) SEM image of a SUS304 substrate without coating which was oxidized at  $900^\circ C$  for 1 h in air.

oxidation, but no exfoliation of film is seen. The granular feature of the coating is similar to the coating surface reported by Shane and Mecartney.<sup>2</sup> Photo (c) is a SEM image of a SUS304 substrate without coating that was oxidized in air. The surface was heavily attacked by oxygen, and the oxidized surface is seen to be swollen.

Figure 5 shows XRD patterns of (a) the oxidized substrate, (b) the substrate with a pure zirconia film that showed a large oxidation weight gain, and (c) the substrate with a  $ZrO_2$ -20 mol%  $YO_{1.5}$  film which showed a small oxidation weight gain. Indexes of  $FeCr_2O_4$  and  $(Fe_{0.6}Cr_{0.4})_2O_3$  were assigned according to Shane and Mecartney.<sup>2</sup> The peak intensities of oxides are seen to become smaller by the addition of  $Y_2O_3$  as compared with the substrates' 111 peak intensities. The relative peak intensities of oxides to the 111 peak intensities of the substrates are plotted in Figs. 6 and 7 as a function of  $Y_2O_3$  content. The 400 and 711 relative peak intensities of  $FeCr_2O_4$  are seen to decrease with increasing  $Y_2O_3$  content. Although the 104 relative peak intensities of  $(Fe_{0.6}Cr_{0.4})_2O_3$  take especially high values at 28 and 30 mol%  $YO_{1.5}$ , they are found to decrease generally in the  $Y_2O_3$  composition less than 26 mol%  $YO_{1.5}$ . These results indicate the decrease of oxide scale thickness by the  $Y_2O_3$  addition and agree with the result of the oxidation weight gain measurement.

### (3) XRD Analysis of the Powders Obtained from the Coating Liquids

Figure 8 shows the X-ray diffraction patterns of zirconia powders obtained from the coating liquids by firing at  $900^\circ C$  for

3 h in air. Peaks of monoclinic and tetragonal phases coexist in Fig. 8(a), but the monoclinic phase decreases quickly with increasing  $Y_2O_3$  content.

Figures 9 and 10 show the lattice constants and cube roots of the unit cell volumes of the tetragonal and cubic phases of the powders as a function of  $Y_2O_3$  content, where the data of the  $ZrO_2$ - $Y_2O_3$  specimens prepared by the rapid cooling from a high temperature are also included.<sup>5</sup> The results of both studies take almost the same values. Figure 11 shows the  $c/a$  ratios of the sol-gel-derived powders and the data plotted according to Yoshimura *et al.*<sup>5</sup> The  $c/a$  ratios of both studies agree well. These facts indicate that the unit cell structure of the sol-gel-derived powders is very close to that of the specimens obtained by the rapid cooling and also the compositional homogeneity of the films prepared by the sol-gel processing. But it will be shown later that the coated films contain a large amount of substrate elements. The  $c/a$  ratio  $y$  of the present study was fitted by the following second-order polynomial for  $ZrO_{2-x}$  mol%  $YO_{1.5}$ .

$$y = 1.019 - 0.0004873x - 0.00004723x^2 \quad (4)$$

The composition that makes  $y = 1$  is the boundary between the tetragonal and cubic phases and is determined as 15.6 mol%  $YO_{1.5}$  (8.5 mol%  $Y_2O_3$ ) by extrapolating the curve to  $y = 1$  (solving Eq. (4)). This value is close to the reported  $c-t$  phase boundary of 8 mol%  $Y_2O_3$  of rapidly cooled specimens.<sup>8</sup> However, the crossing point that is obtained by the linear extrapolation of  $c$  and  $a$  axes gives 19.3 mol%  $YO_{1.5}$  (10.7 mol%  $Y_2O_3$ , Fig. 9), which is far beyond the above value.

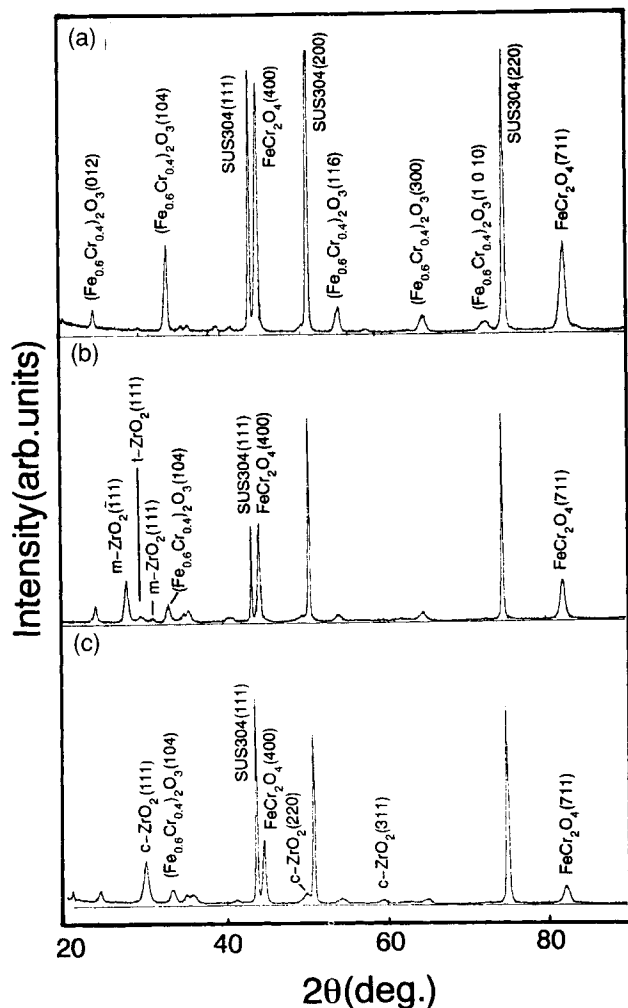


Fig. 5. XRD patterns of the specimens after the oxidation experiment at 900°C for 1 h: (a) substrate without coating, (b) substrate with a pure  $\text{ZrO}_2$  film, (c) substrate with a  $\text{ZrO}_2$ -20 mol%  $\text{YO}_{1.5}$  film.

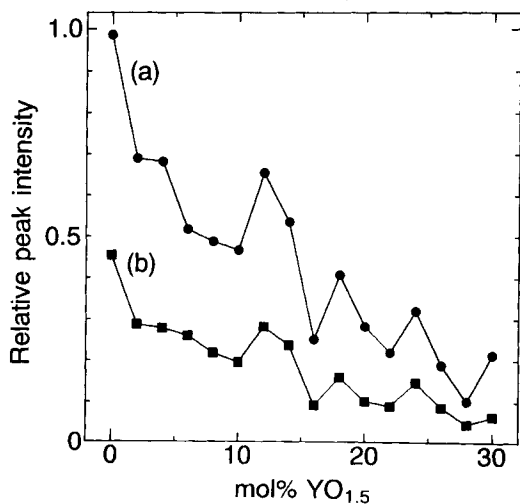


Fig. 6. Relative XRD peak intensities of  $\text{FeCr}_2\text{O}_4$  against the substrates' 111 peak intensities as a function of  $\text{Y}_2\text{O}_3$  content: (a) 400 reflection, (b) 711 reflection.

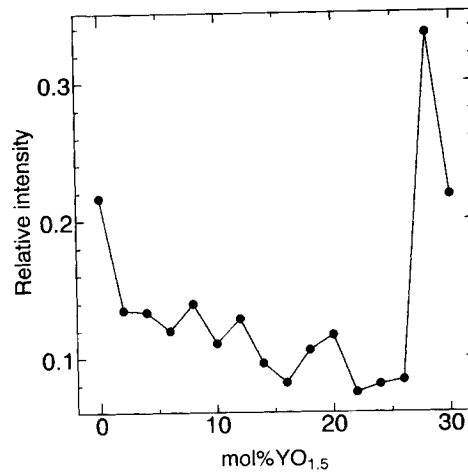


Fig. 7. 104 relative XRD peak intensities of  $(\text{Fe}_{0.6}\text{Cr}_{0.4})_2\text{O}_3$  against the substrates' 111 peak intensities as a function of  $\text{Y}_2\text{O}_3$  content.

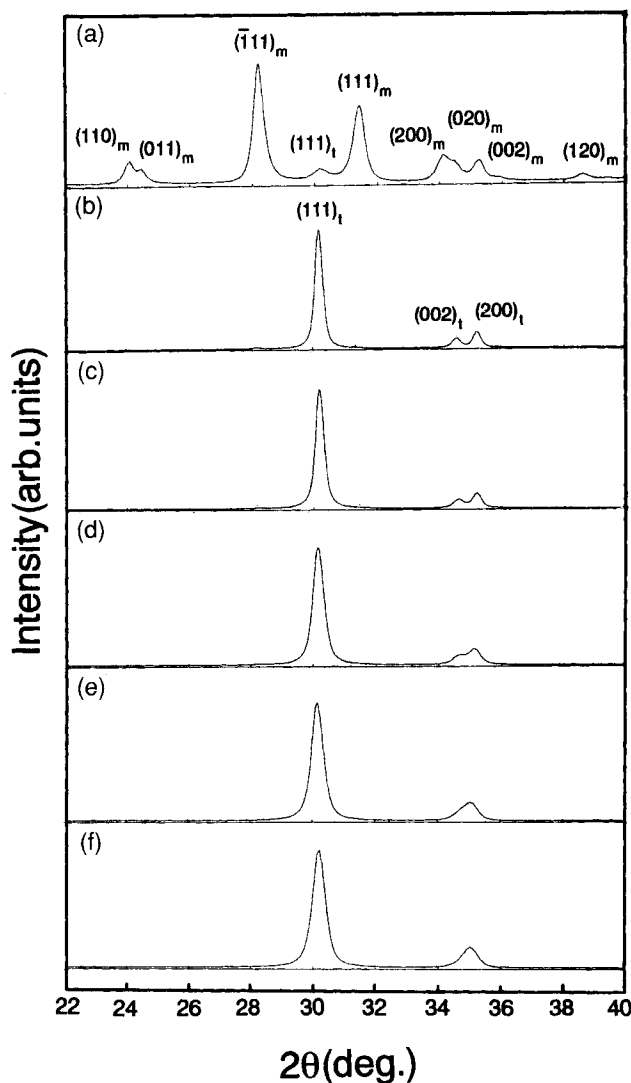


Fig. 8. X-ray diffraction patterns of the sol-gel-derived  $\text{ZrO}_2$ - $\text{Y}_2\text{O}_3$  powders obtained from the coating liquids by firing at 900°C for 3 h in air: (a)  $\text{ZrO}_2$ -0 mol%  $\text{YO}_{1.5}$ , (b)  $\text{ZrO}_2$ -2 mol%  $\text{YO}_{1.5}$ , (c)  $\text{ZrO}_2$ -4 mol%  $\text{YO}_{1.5}$ , (d)  $\text{ZrO}_2$ -6 mol%  $\text{YO}_{1.5}$ , (e)  $\text{ZrO}_2$ -8 mol%  $\text{YO}_{1.5}$ , (f)  $\text{ZrO}_2$ -10 mol%  $\text{YO}_{1.5}$ .

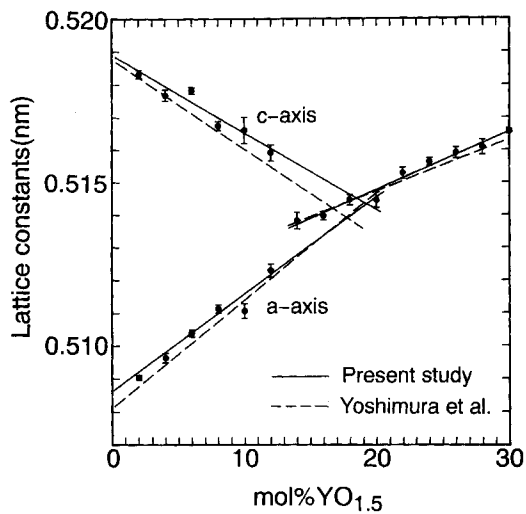


Fig. 9. Lattice constants of the tetragonal and cubic phases of the sol-gel-derived  $ZrO_2$ - $Y_2O_3$  powders and the specimens obtained by rapid cooling from a high temperature (Yoshimura *et al.*<sup>4</sup>).

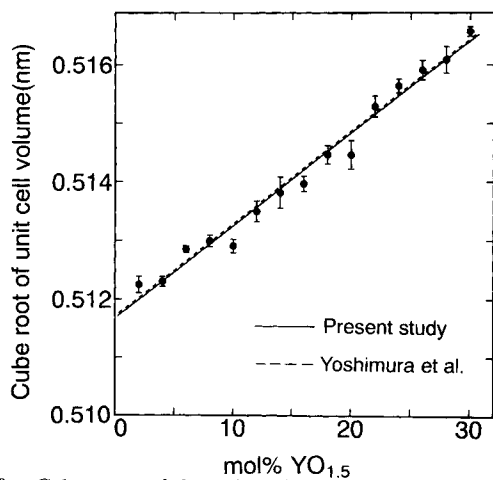


Fig. 10. Cube roots of the unit cell volumes in the tetragonal and cubic phases of the sol-gel-derived  $ZrO_2$ - $Y_2O_3$  powders and the data by Yoshimura *et al.*<sup>4</sup>

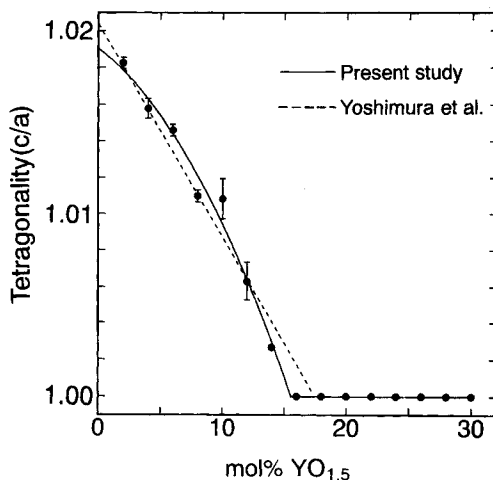


Fig. 11.  $c/a$  ratios of the sol-gel-derived  $ZrO_2$ - $Y_2O_3$  powders and the data by Yoshimura *et al.*<sup>4</sup>

(4) Comparison between the Films Subjected to the Oxidation Experiment and the Sol-Gel-Derived Powders by XRD Analysis

Figure 12 shows the X-ray diffraction patterns around 111 reflections of the films after the oxidation experiment. The monoclinic phase is seen to decrease with increasing  $Y_2O_3$  content which is similar to Fig. 8. Figure 13 shows the ratios of the integrated intensity of the monoclinic phase plotted against the total intensity of the monoclinic and tetragonal phases of the films and the powders. The ratios of the integrated intensity are calculated for 111 reflections as  $(I_{m\bar{1}11} + I_{m111}) / (I_{m\bar{1}11} + I_{m111} + I_{t111})$  according to Kimura *et al.*<sup>9</sup> Tetragonal phase is seen to disappear more quickly in the films than in the powders with decreasing  $Y_2O_3$  content. This result indicates that the tetragonal phase of the films is less stable than in the powders. This is considered to have been caused by the thermal stress that occurred through the bonding and oxidation experiments.

The (111) plane spacings of the tetragonal and cubic phases of the films and the powders are plotted as a function of  $Y_2O_3$  content in Fig. 14. The plane spacings of the films take larger values than the powders.

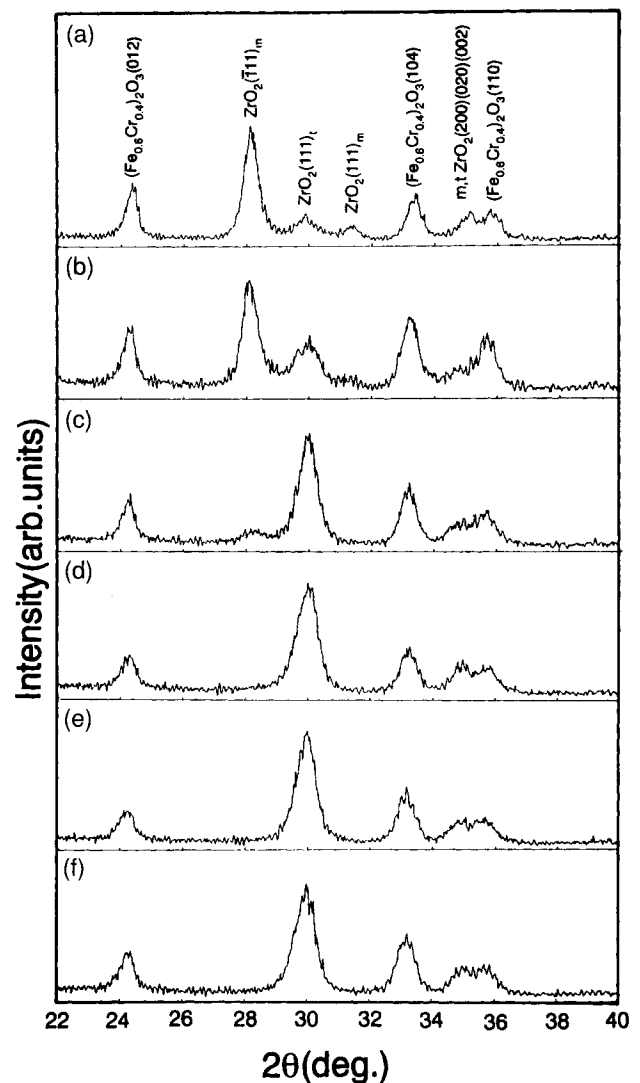
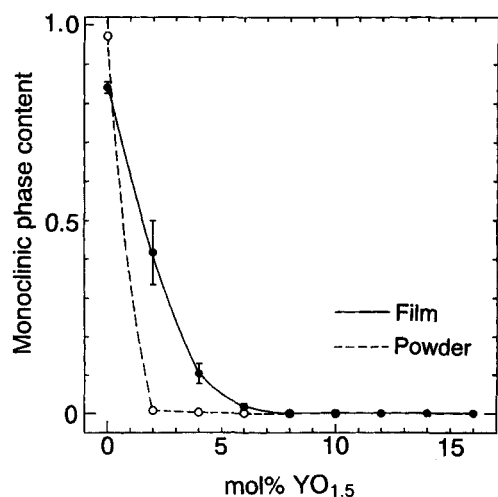


Fig. 12. X-ray diffraction patterns around the 111 reflections of the coatings after the oxidation experiment: (a)  $ZrO_2$ -0 mol%  $YO_{1.5}$ , (b)  $ZrO_2$ -2 mol%  $YO_{1.5}$ , (c)  $ZrO_2$ -4 mol%  $YO_{1.5}$ , (d)  $ZrO_2$ -6 mol%  $YO_{1.5}$ , (e)  $ZrO_2$ -8 mol%  $YO_{1.5}$ , (f)  $ZrO_2$ -10 mol%  $YO_{1.5}$ .



**Fig. 13.** Ratios of the 111 integrated intensities of the monoclinic phase against the total 111 integrated intensities of the monoclinic and tetragonal phases of the films and the powders obtained from the coating liquids.

#### (5) TEM Observation of the Films and Joint Interfaces

Figure 15 shows a cross-sectional observation of the interface between the ZrO<sub>2</sub>-15 mol% YO<sub>1.5</sub> film and SUS304 substrate which was prepared by firing at 900°C for 2 h under vacuum. An intermediate layer is seen to be formed in the dark-field observation where the contrast of the layer is bright along the interface. This bright contrast, which did not change by tilting the specimen in the observation, indicates that the intermediate layer is amorphous. In order to confirm this point, a high-resolution image (Fig. 16) around the marked place was taken. The image clearly shows the existence of an amorphous phase. The layer thickness was observed to be approximately 10 to 50 nm. Figure 17 shows a HRTEM image of a ZrO<sub>2</sub>-15 mol% YO<sub>1.5</sub> film prepared by firing at 600°C for 2 h. An intermediate layer is shown to be formed at the marked place, but the layer width is seen to be reduced. In Fig. 18, which is of a pure zirconia film prepared at 900°C for 2 h in vacuum, the width of the intermediate layer is seen to be reduced also and cannot be seen clearly. These facts indicate that addition of Y<sub>2</sub>O<sub>3</sub> and elevation of firing temperature help the formation of the intermediate layer. EDX analyses of the films, film-substrate interfaces, and substrates are shown in Figs. 19, 20, and 21. These figures

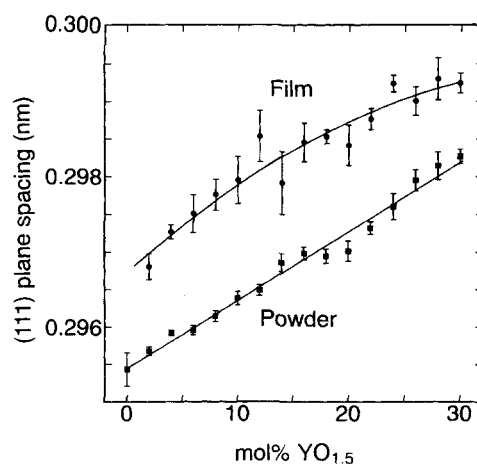


**Fig. 14.** (111) plane spacings of the tetragonal and cubic phases of the coated films and the powders.

show that the elements of stainless steel, Fe, Ni, and Cr are contained in the films. By using the program of standardless quantitative analysis, the film composition was roughly estimated in atomic percentage as Zr:Fe:Cr = 74.7:10.6:10.7 in the ZrO<sub>2</sub>-15 mol% YO<sub>1.5</sub> (8 mol% YO<sub>1.5</sub>) film (Fig. 15) and 72.1:20.1:7.8 in the ZrO<sub>2</sub>-0 mol% Y<sub>2</sub>O<sub>3</sub> film (Fig. 18).

At the film-substrate interface of ZrO<sub>2</sub>-15 mol% YO<sub>1.5</sub> film (Fig. 19(b)), a strong peak of Si is seen. As shown in Fig. 19(c) where a small peak of Si is detected in the substrate, the SUS304 stainless steel on the market generally contains about 1 mass% Si as an impurity.<sup>12</sup> The concentrated Si at the film-substrate interface must have been accumulated from the inner part of the substrate. The Si peak can be seen also in Fig. 20(b), but is not so strong as compared with Fig. 19(b). This fact supports that addition of Y<sub>2</sub>O<sub>3</sub> enhances the segregation of Si and is consistent with the HRTEM observations. In Fig. 21(b), the peak of Si is much weaker than in Fig. 19(b). Elevation of firing temperature is found to help the accumulation of Si.

#### IV. Discussion

The thermal expansion coefficient of zirconia is reported to be  $(9.33-11.08) \times 10^{-6}/^{\circ}\text{C}$  for single-crystal ZrO<sub>2</sub>-(3-20 wt%) Y<sub>2</sub>O<sub>3</sub> in the temperature range 20°-1500°C, while that of stainless steels is  $14.7 \times 10^{-6}/^{\circ}\text{C}$  (20°C) -  $20.2 \times 10^{-6}/^{\circ}\text{C}$

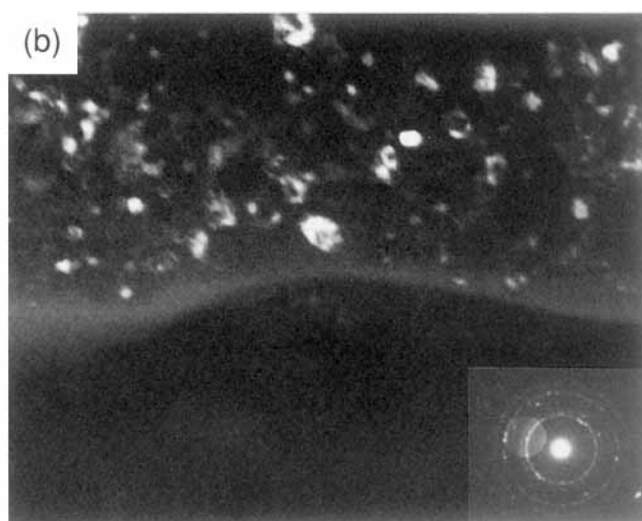
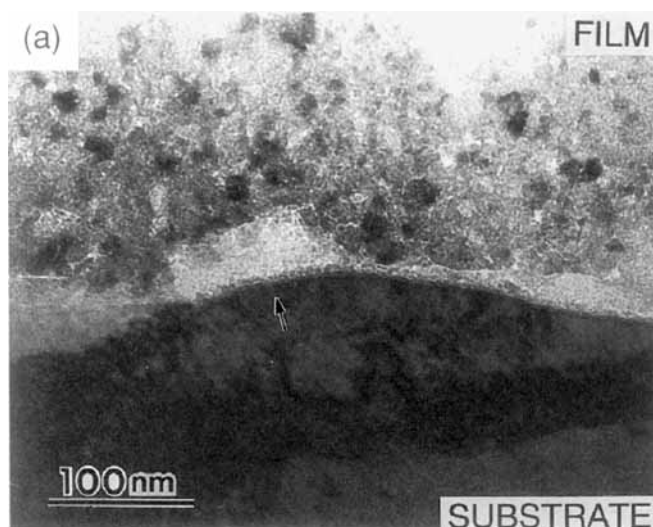


**Fig. 15.** Cross-sectional TEM images of the interface between the ZrO<sub>2</sub>-15 mol% YO<sub>1.5</sub> film and SUS304 substrate prepared by firing at 900°C for 2 h under vacuum: (a) bright-field image, (b) dark-field image by the diffraction spots shown with an image of the aperture.

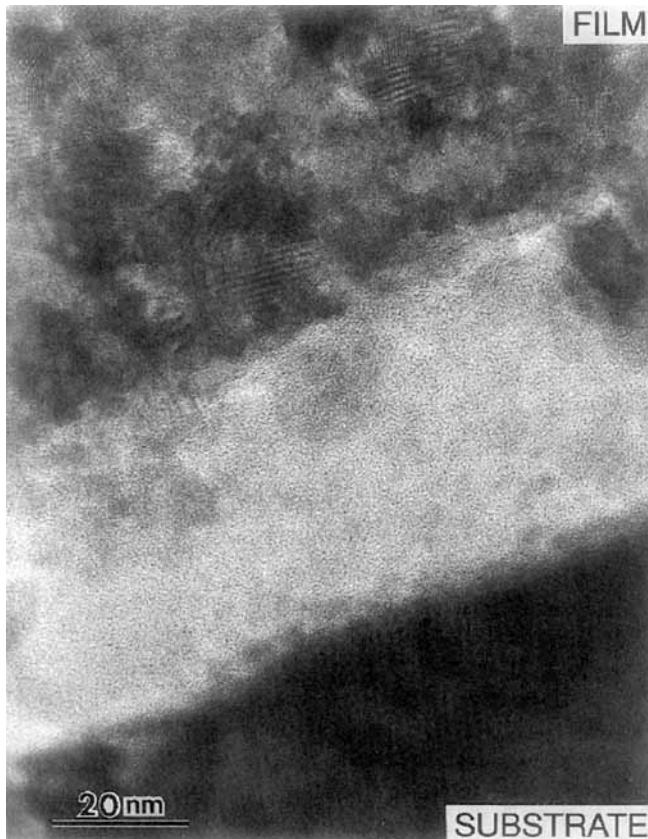


**Fig. 16.** Cross-sectional HRTEM image around the marked place of Fig. 15. An amorphous intermediate layer is observed.

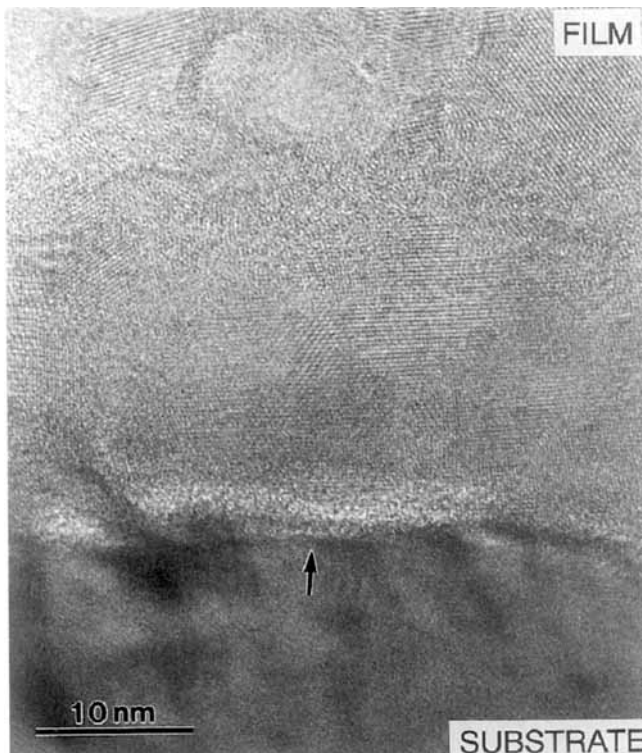


**Fig. 17.** Cross-sectional HRTEM image of the interface between the  $ZrO_2$ -15 mol%  $YO_{1.5}$  film and SUS304 substrate prepared by firing at  $600^\circ\text{C}$  for 2 h.

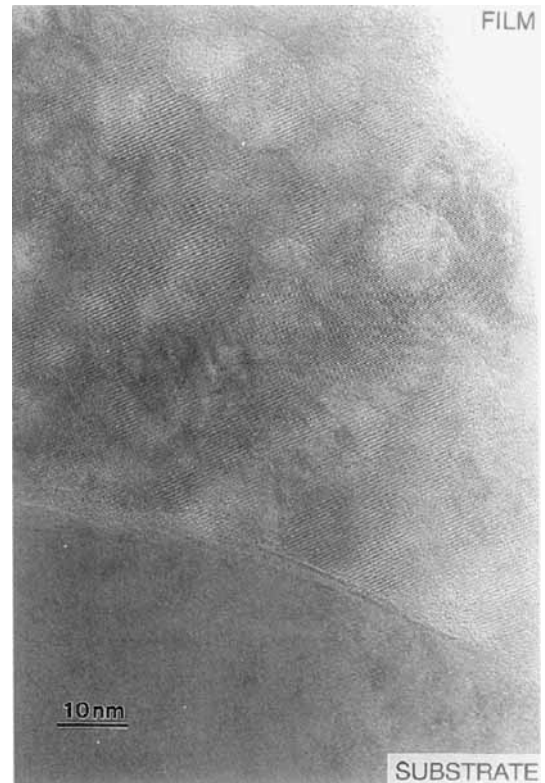


**Fig. 18.** Cross-sectional HRTEM image of the interface between the pure  $ZrO_2$  film and substrate prepared by firing at  $900^\circ\text{C}$  for 2 h under vacuum.

( $527^\circ\text{C}$ ).<sup>10,11</sup> The thermal expansion coefficient of stainless steel is fairly close to that of zirconia, but it does not exactly coincide. Therefore, the thermal stress at the film-substrate interface is inevitably generated by the heat treatment. This thermal stress will make the film shrink, but the (111) plane spacings of the films were found to be expanded, compared with those of the powders. The TEM-EDX analyses showed that a large amount of the substrate's elements, Fe and Cr, were contained in the films. Fe and Cr are considered to exist as  $Fe^{3+}$  or  $Cr^{3+}$  in a thin film. The ion radii of  $Fe^{3+}$ ,  $Cr^{3+}$ ,  $Zr^{4+}$ ,  $Y^{3+}$ , and  $O^{2-}$  are reported to be 0.064–0.067 nm, 0.063–0.065 nm, 0.079–0.087 nm, 0.092–0.106 nm, and 0.132–0.14 nm, respectively.<sup>13</sup> If the cation sites are substituted by  $Fe^{3+}$  and  $Cr^{3+}$  whose ion radii are smaller than  $Zr^{4+}$  or  $Y^{3+}$ , the lattice constants must become smaller according to the spherical ion packing model.<sup>7</sup> Therefore, the expansion of a unit cell of the films is considered to be explained by assuming the interstitial type solid solution of iron or chromium oxides into the films. Shane and McCartney<sup>2</sup> reported that an interfacial reaction between the sol-gel-derived  $ZrO_2$ -8 wt%  $Y_2O_3$  film and the stainless steel substrate formed iron chromates which led to the strong interfacial bonding and that the amount of iron chromates increased by elevating heat treatment temperature. But in the present experiment, though the iron chromates were identified,  $ZrO_2$ - $Y_2O_3$  films were joined to the stainless steel substrates via an amorphous oxide layer with concentrated Si, and this oxide layer was found to grow thicker by adding  $Y_2O_3$  or by elevating the firing temperature. Presumably, this amorphous oxidation layer will behave as a glass solder which helps the bonding by relaxing the thermal stress during the heat treatment in addition to the strengthening by the iron chromates. This glass layer is expected to improve the oxidation resistance partly, since De Sanctis *et al.*<sup>14</sup> have shown that a sol-gel-derived  $SiO_2$  film with a thickness of  $0.4\ \mu\text{m}$  worked effectively to limit the oxidation of stainless steel.

As shown in Figs. 6 and 7, the relative peak intensities of  $FeCr_2O_4$  (400, 711) and  $(Fe_{0.6}Cr_{0.4})_2O_3$  (104) against the 111

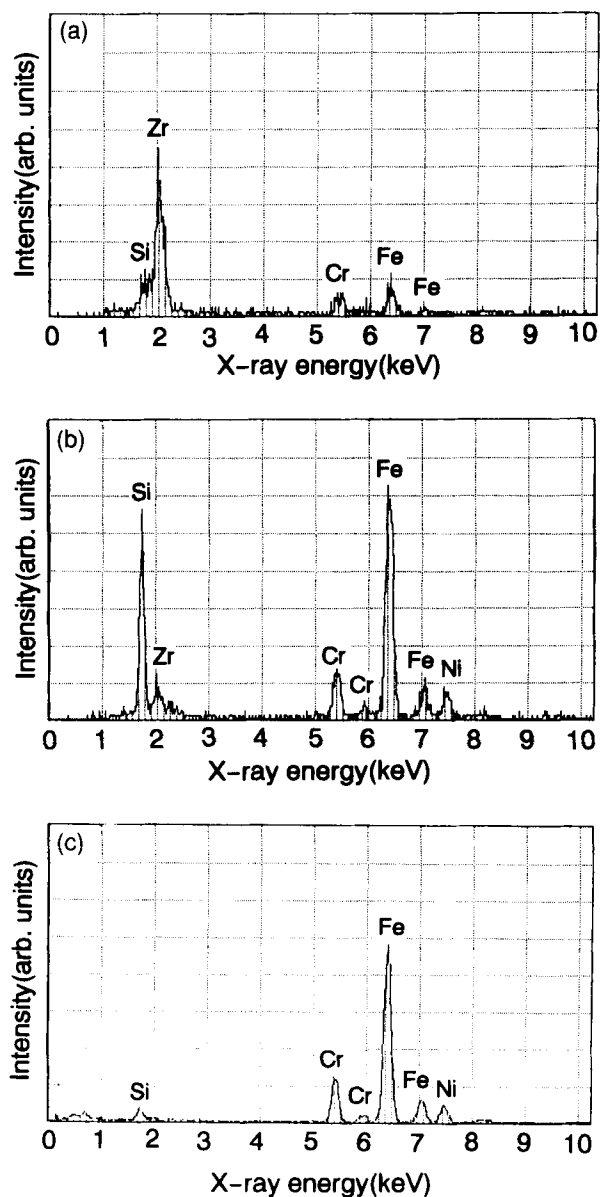


Fig. 19. EDX analyses of (a) the film (109 nm apart from the film-substrate interface), (b) the film-substrate interface, and (c) the substrate (50 nm inward from the interface) in the specimen of Fig. 15.

peak intensities of the SUS304 substrates were found to decrease with increasing  $Y_2O_3$  content; i.e., addition of  $Y_2O_3$  to the films prevented the formation of oxides. The 400 peaks of  $FeCr_2O_4$  are especially high in Fig. 5. This fact suggests that (400) planes of  $FeCr_2O_4$  crystals are oriented in parallel with the substrate surface. In Fig. 6, the  $FeCr_2O_4$  711 peaks seem to have a correlation with 400 peaks in intensity. In order to examine this, the 711 relative peak intensities were plotted against the 400 relative peak intensities, as shown in Fig. 22. Figure 22 shows the strong correlation between the 400 and 711 peak intensities. This result supports the orientation of (400) planes parallel to the substrate surface, because the (711) planes are the lattice planes whose orientation is close to the (400) planes. Since the (400) plane spacing of  $FeCr_2O_4$  (0.20943 nm) is similar to the (111) plane spacing of the substrate (0.21 nm), the  $FeCr_2O_4$  (400) and SUS304 (111) planes are considered to have an epitaxial relationship. Presumably, the stainless steel substrates have a texture, and the (400) planes of  $FeCr_2O_4$  must have nucleated in parallel with the substrates' (111) planes.

It has been shown by Izumi *et al.*<sup>1</sup> that the oxidation weight gain can be reduced by increasing  $ZrO_2$  coating thickness.

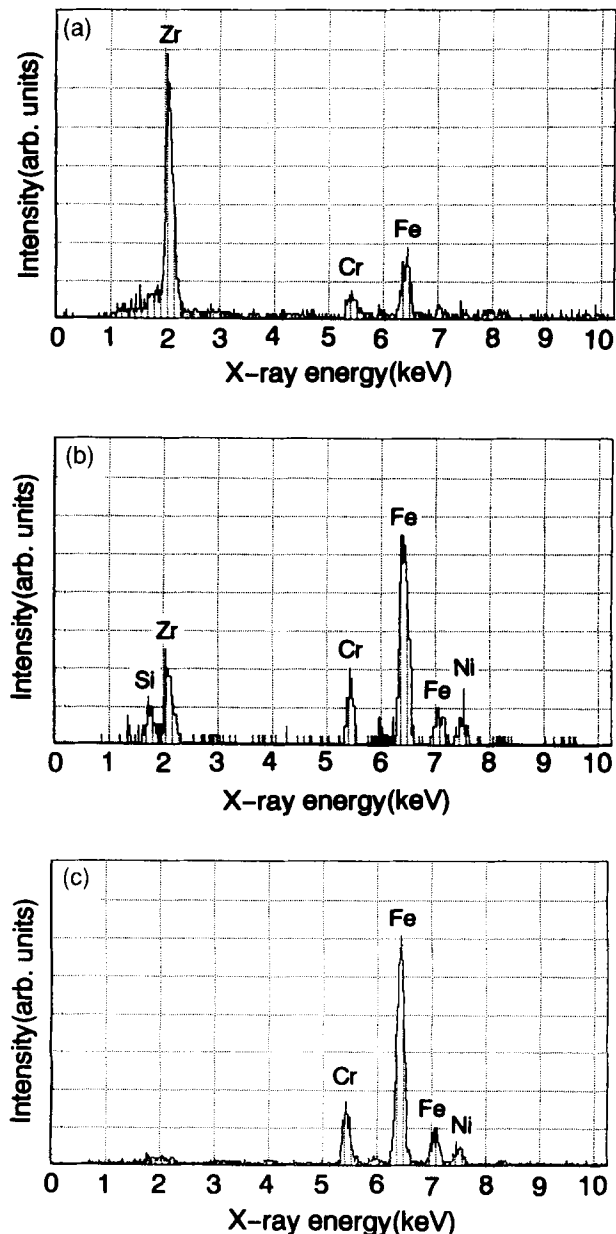


Fig. 20. EDX analyses of (a) the film (65 nm apart from the interface), (b) the film-substrate interface, and (c) the substrate (8 nm inward from the interface) in the specimen of Fig. 18.

Figure 2 indicates that the film thickness increases for  $Y_2O_3$  content less than 14 mol%  $YO_{1.5}$ . The reduction of oxidation weight gain in the smaller  $Y_2O_3$  content region of the present study may be explained by the increase of film thickness. The oxidation weight gain, however, decreased generally with increasing  $Y_2O_3$  content (Fig. 3), though the film thickness was found to decrease in the higher  $Y_2O_3$  content region. This shows that the reduction of oxidation weight gain by  $Y_2O_3$  addition cannot be explained by the variation of film thickness. It is said that  $Y_2O_3$  exhibits a strong affinity for oxygen and is very effective in trapping the impurity oxygen from the matrix of ceramics such as AlN.<sup>15</sup> Therefore, addition of  $Y_2O_3$  to zirconia films is considered to have suppressed the oxidation of substrates by trapping the oxygen ions around  $Y^{3+}$  ions. Since the addition of yttrium is known to improve the oxidation resistance of Fe-Cr base alloys,<sup>16</sup> the diffusion of yttrium from the coating into the substrate may contribute to the oxidation resistance. This factor is to be investigated further.

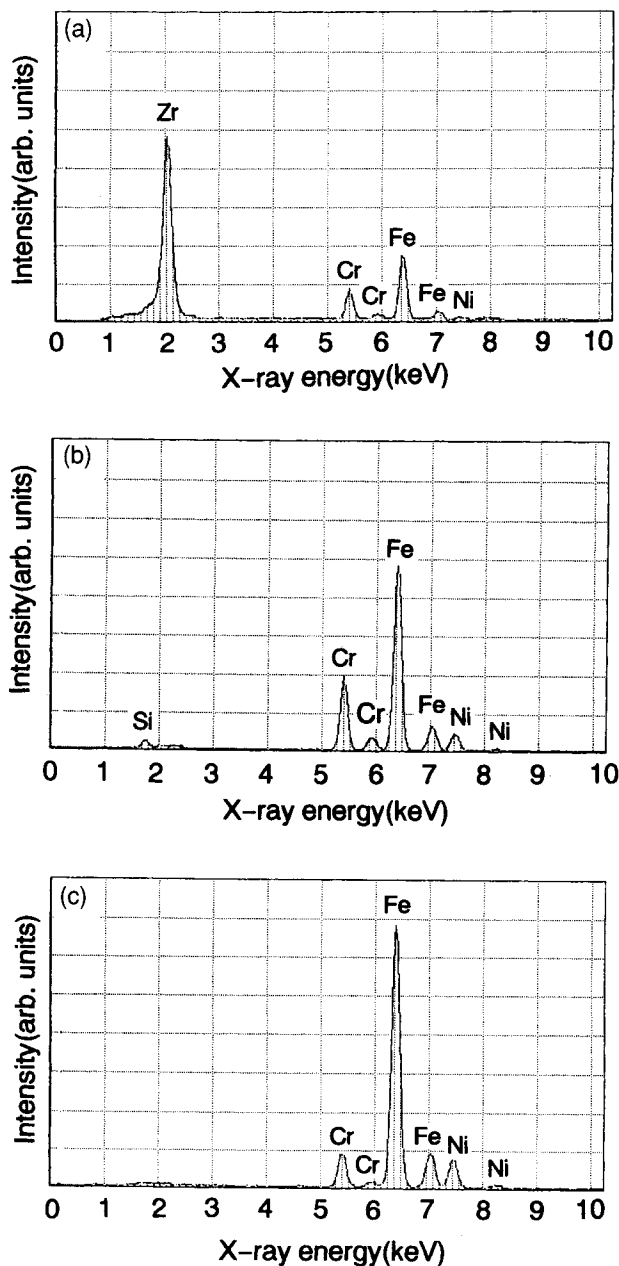


Fig. 21. EDX analyses of (a) the film (64 nm apart from the interface), (b) the film-substrate interface, and (c) the substrate (68 nm inward from the interface) in the specimen of Fig. 17.

## V. Conclusions

This study is summarized as follows.

- (1) The oxidation resistance of stainless steel substrates with sol-gel-derived  $ZrO_2$ - $Y_2O_3$  films can be improved by increasing  $Y_2O_3$  content.
- (2) At the film-substrate interface, a thin amorphous oxide layer rich in Si is formed. The layer thickness increased by the addition of  $Y_2O_3$ . The intermediate layer is considered to behave as a glass solder which joins the film and the substrate.
- (3) The (111) lattice plane spacings of the films take larger values than those of the powders obtained from the coating liquids, due to the diffusion of the substrate's elements into the films.
- (4) More monoclinic phase was found to be formed in the films than in the powders having the same  $Y_2O_3$  content. This indicates that the tetragonal-to-monoclinic phase transformation of zirconia took place more easily in the films through the bonding and oxidation process.

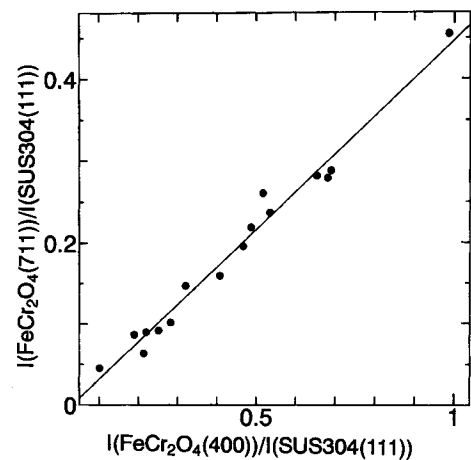


Fig. 22. Relationship between the 400 and 711 XRD peak intensities ( $I$ ) of  $FeCr_2O_4$ . The intensities are shown as the relative values against the 111 peak intensities of the SUS304 substrates.

- (5) The lattice constants and  $c/a$  ratios of the tetragonal phase and cube roots of the unit cell volumes of the tetragonal and cubic phases of  $ZrO_2$ - $Y_2O_3$  powders obtained from the coating liquids are very close to those of  $ZrO_2$ - $Y_2O_3$  specimens rapidly cooled from a high temperature. This is an indication of the close structural resemblance between the sol-gel-derived powders and the specimens formed by the rapid cooling, and the compositional homogeneity of the sol-gel-derived powders.

**Acknowledgments:** We are very grateful to Professors T. Sakuma and Y. Ishida (University of Tokyo) for valuable discussions, Professor S. Takeuchi and Mr. M. Nakamura (University of Tokyo) for the studies by HRTEM, ESCA, and EPMA, and to Mr. K. Itoi and Mr. R. Matoba (University of Tokyo) for assistance in the specimen preparation and oxidation experiment.

## References

- <sup>1</sup>K. Izumi, M. Murakami, T. Deguchi, A. Morita, N. Tohge, and T. Minami, "Zirconia Coating on Stainless Steel Sheets from Organozirconium Compounds," *J. Am. Ceram. Soc.*, **72** [8] 1465-68 (1989).
- <sup>2</sup>M. Shane and M. L. Mecartney, "Sol-Gel Synthesis of Zirconia Barrier Coatings," *J. Mater. Sci.*, **25** [3] 1537-44 (1990).
- <sup>3</sup>J. F. Baumard and P. Abelard, "Defect Structure and Transport Properties of  $ZrO_2$ -Based Solid Electrolytes"; pp. 555-71 in *Advances in Ceramics*, Vol. 12, *Science and Technology of Zirconia II*, Edited by C. Clausen, M. Rühle, and A. H. Heuer. American Ceramic Society, Columbus, OH, 1984.
- <sup>4</sup>J. M. Bennett and J. H. Dancy, "Stylus Profiling Instrument for Measuring Structural Properties of Smooth Optical Surfaces," *Appl. Opt.*, **20** [10] 1785-802 (1981).
- <sup>5</sup>M. Yoshimura, M. Yashima, T. Noma, and S. Somyia, "Formation of Diffusionlessly Transformed Tetragonal Phases by Rapid Quenching of Melts in  $ZrO_2$ - $RO_{1.5}$  Systems (R = Rare Earths)," *J. Mater. Sci.*, **25** [4] 2011-16 (1990).
- <sup>6</sup>L. H. Schwartz and J. B. Cohen, *Diffraction from Materials*, 2nd ed.; p. 224. Springer-Verlag, Berlin, Germany, 1987.
- <sup>7</sup>R. P. Ingel and D. Lewis III, "Lattice Parameters and Density for  $Y_2O_3$ -Stabilized  $ZrO_2$ ," *J. Am. Ceram. Soc.*, **69** [4] 325-32 (1986).
- <sup>8</sup>T. Sakuma and H. Hata, "Diffusionless Cubic-to-Tetragonal Transformation and Microstructure in  $ZrO_2$ - $Y_2O_3$ ," *J. Jpn. Inst. Met.*, **53** [9] 972-79 (1989).
- <sup>9</sup>N. Kimura, H. Okamura, and J. Morishita, "Preparation of Low- $Y_2O_3$ -TZP by Low-Temperature Sintering"; pp. 183-91 in *Advances in Ceramics*, Vol. 24, *Science and Technology of Zirconia III*, Edited by S. Somyia, N. Yamamoto, and H. Yanagida. American Ceramic Society, Columbus, OH, 1986.
- <sup>10</sup>J. W. Adams, H. H. Nakamura, R. P. Ingel, and R. W. Rice, "Thermal Expansion Behavior of Single-Crystal Zirconia," *J. Am. Ceram. Soc.*, **68** [9] C-228-C-231 (1985).
- <sup>11</sup>Chronological Scientific Tables; p. 470. Edited by National Astronomical Observatory. Maruzen, Tokyo, Japan, 1992.
- <sup>12</sup>Japanese Industrial Standard Survey of Steels, JIS G 4304, Vol. 2, p. 816. Shin-nihon Hoki Publishing Co., Japan, 1992.
- <sup>13</sup>F. S. Galasso, *Structure and Properties of Inorganic Solids*. Pergamon Press, Elmsford, NY, 1970.
- <sup>14</sup>O. De Sanctis, L. Gomez, and N. Pellegrini, "Protective Glass Coatings on Metallic Substrates," *J. Non-Cryst. Solids*, **121**, 338-43 (1990).
- <sup>15</sup>H. Yanagida, "Consulting Periodic Tables for Research and Development of Functional Ceramics," *Met. Technol.*, **58** [9] 41-45 (1988).
- <sup>16</sup>D. P. Whittle and J. Stringer, "Improvements in High Temperature Oxidation Resistance by Additions of Reactive Elements or Oxide Dispersions," *Philos. Trans. R. Soc. London, A*, **295** [1413] 309-29 (1980). □